Journal of Photochemistry & Photobiology A: Chemistry 383 (2019) 112026

Contents lists available at ScienceDirect

Journal of Photochemistry & Photobiology A: Chemistry

journal homepage: www.elsevier.com/locate/jphotochem

A simple fluorescent schiff base for sequential detection of Zn^{2+} and PPi based on imidazo[2,1-*b*]thiazole

Yuankang Xu[a], Hanyu Wang[a], Jinyan Zhao[b], Xiaofeng Yang[a], Meishan Pei[a], Guangyou Zhang[a], Yanxia Zhang[a,*], Li Lin[c,*]

[a] School of Chemistry and Chemical Engineering, University of Jinan, Jinan 250022, China
[b] Jinan Technician College, China
[c] College of Science, Sichuan Agricultural University, China

ARTICLE INFO

Keywords:
Schiff base
Zinc
PPi
Detection limit
Theoretical calculations
Logic circuit

ABSTRACT

A simple fluorescent schiff base, **X**, based on imidazo[2,1-*b*]thiazole-6-carboxylic acid and 3-ethoxy-2-hydroxybenzaldehyde, was designed and synthesized for detection of Zn^{2+} and PPi. **X** showed excellent sensitivity and selectivity toward Zn^{2+} by exhibiting a large fluorescence enhancement (about 42 times). The binding ratio of the **X** and Zn^{2+} was 1:1 confirmed by mass spectral analysis and Job's plot and the association constant between **X** and Zn^{2+} was calculated to be 2.2×10^5 M^{-1}. The detection limit was as low as 1.2×10^{-9} M. Moreover, the **X**[Zn^{2+}] complex could be used as a sensor to detect PPi sensitively and the detection limit was 1.9×10^{-9} M. Furthermore, the fluorescent signals of **X** were utilized to construct an INHIBIT logic gate at the molecular level. The reason of fluorescence enhancement of **X** toward Zn^{2+} was verified by density functional theory (DFT) and time-dependent density functional theory (TDDFT) calculations using Gaussian 09.

1. Introduction

At the present, detection of transition metals in environmental and biological has attracted increasing attention due to their important role in the system [1,2]. Among the various transition metals, zinc, as one of the essential trace elements in human body, is the second most abundant transition element in the body and is involved in a variety of metabolic and physiological processes, such as gene transcription/expression, cell growth and division, neurotransmission and mammalian reproduction [3–6]. Minute quantity of zinc is beneficial to human body, on the other hand, the excessive zinc will damage the human body's function, such as Alzheimer's disease and Parkinson's disease [7–10]. Among the various anions, pyrophosphate ($P_2O_7^{4-}$, PPi) is an important anion in many physiological processes, such as cellular ATP hydrolysis, protein synthesis, DNA and RNA polymerizations, enzymatic reactions and other metabolic processes [11–13]. However, an excess of PPi can cause calcium pyrophosphate deposition disease (CPPD) and other diseases [14]. Hence, efficient recognition of zinc and pyrophosphate is of great significance to biology, clinical medicine and other fields.

Nowadays, more and more attention has been paid on fluorescence analysis rather than traditional detection methods because of its good selectivity, high sensitivity, simple operation and other characteristics [15–17]. Among many reported fluorescent probes for zinc, schiff bases have attracted much attention due to their simple synthesis, good solubility and strong complexing capacity [18–21]. Detection of zinc are often affected by other metallic ions, such as chromium, which have similar properties [22,23]. In addition, the content of zinc in human body is around 1.96 ~ 5.34×10^{-6} mol L^{-1} [17]. Therefore, the design and synthesis of a schiff base with simple structure as a fluorescent probe for highly selective and sensitive of zinc is continuously to be a challengeable work.

In this report, a new simple schiff base (**X**) was designed and synthesized based on imidazo[2,1-*b*]thiazole-6-carboxylic acid and 3-ethoxy-2-hydroxybenzaldehyde. imidazo[2,1-*b*]thiazole, which contains two conjugated rings in its molecule, contains eight central atoms at the heterocyclic rings with ten delocalized π electrons, was a potential fluorescent nucleus [24]. Moreover, imidazo[2,1-*b*]thiazole ring has two nitrogen atoms and one sulfur atom, which provides a possibility for coordination of metal ions [25]. On the other hand, 3-ethoxy-2-hydroxybenzaldehyde, as fluorescence receptor, are connected with fluorescence nuclei by C=N bond in the probe molecule. In addition, the hydroxyl and ethoxy groups on the benzene ring can not only increase the ability of the probe to recognize ions, but also greatly

* Corresponding authors.
E-mail addresses: chm_zhangyx@ujn.edu.cn (Y. Zhang), 14211@sicau.edu.cn (L. Lin).

https://doi.org/10.1016/j.jphotochem.2019.112026
Received 22 May 2019; Received in revised form 16 July 2019; Accepted 7 August 2019
Available online 07 August 2019
1010-6030/

improve the solubility of the probe. As expected, compound **X** could be used as a highly selective and sensitive fluorescent probe to detect zinc ions in ethanol-water buffer system. Furthermore, the combination of probe **X** and zinc ions can serve as a sensor for PPi detection in the same system.

2. Experimental section

2.1. Materials and sample preparation

All reagents and solvents were commercially available AR and CP and were used without any treatment. All metal ionic solution are corresponding chloride or sulfate solutions, including $ZnCl_2$, Li_2SO_4, $AlCl_3{\cdot}6H_2O$, $CdCl_2{\cdot}2.5H_2O$, $CoCl_2{\cdot}6H_2O$, $FeCl_3$, $MgCl_2{\cdot}6H_2O$, $CrCl_3{\cdot}6H_2O$, $MnCl_2{\cdot}4H_2O$, NaCl, $FeSO_4$, KCl, $CuCl_2{\cdot}2H_2O$, $NiCl_2{\cdot}6H_2O$, $CaCl_2$ and $HgCl_2$. All anionic solutions are corresponding sodium or potassium solutions, including $Na_4P_2O_7$, NaCl, NaF, NaBr, KI, $NaNO_2$, $NaHCO_3$, Na_2S, NaS_2O_3, Na_2SO_4, $NaNO_3$, $NaHSO_3$ and $NaBF_3$. Stock solutions of the ions mentioned above were prepared with a concentration of 0.03 M by distilled water. The stock solution of $ZnCl_2$ was diluted to different concentration as 1×10^{-6} M, 1×10^{-7} M, 1×10^{-8} M and was used for the titration test. Similar, the stock solution of PPi was diluted to different concentration as 1×10^{-6} M, 1×10^{-7} M. The probe **X** was dissolved in ethanol/H_2O (v/v = 9 : 1) buffer solution (10 mM tris, pH = 7.4) at room temperature with the concentration of 1×10^{-5} M.

2.2. Measurements

UV-vis spectra were obtained on a Shimadzu 3100 spectrometer. Fluorescence spectral data was recorded on an Edinburgh Instruments Ltd-FLS920 Fluorescence Spectrophotometer. Fluorescence measurements were recorded using excitation at 330 nm. The slits of excitation and emission were 10 nm and 20 nm, respectively. ^{1}H NMR measurement was performed on a Bruker AV III 400 MHz NMR spectrometer. ^{13}C NMR spectra data was taken on a Bruker AV III 100 MHz NMR spectrometer with tatramethysilane (TMS) as internal standard and DMSO as solvent. Infrared spectral data was obtained on a Bruker Vertex 70 FT-IR spectrometer using samples as KBr pellets. Thin layer chromatography (TLC) analyses were performed to monitor all the reactions.

2.3. Calculation of quantum yield and association constant

Quantum yield was calculated according to the following formula (1):

$$\Phi_u = \Phi_s \frac{F_u A_s n_u^2}{F_s A_u n_s^2} \tag{1}$$

Φ, F, A, and n represent the quantum yield, the integrated area under the corrected emission spectra, the absorbance intensity at the excitation wavelength and the refractive index of solvent, respectively. In addition, s refers to rhodamine B as the standard, and u refers to the target. The quantum yield (Φ) of rhodamine B dissolved in anhydrous ethanol is 0.97.

The association constant between **X** and Zn^{2+} was calculated by the Benesi–Hildebrand Eq. (2):

$$\frac{1}{F - F_0} = \frac{1}{Zn^{2+}} \times \frac{1}{K_a[F_{max} - F_0]} + \frac{1}{F_{max} - F_0} \tag{2}$$

where F is the fluorescence intensity of the **X**-Zn^{2+} complex, which is in accordance with the concentration of Zn^{2+} at 511 nm. F_0 is the fluorescence intensity of free **X**. Fmax is the fluorescence intensity of **X**-Zn^{2+} complex in the presence of the maximum concentration of Zn^{2+}.

2.4. Theoretical calculations

Density functional theory (DFT) structural optimizations were performed with the Gaussian 09 program. In all cases, the structures were optimized using the B3LYP functional and the mixed basis set 6-31 + G (d). Each structure was subsequently subjected to TD-DFT calculation using the B3LYP functional [26]. For all optimized structures, frequency calculations were performed to confirm the absence of imaginary frequencies. The molecular orbitals were visualized and plotted with the GaussView 5.0 program.

2.5. Synthesis of X

Compound **1** (ethyl imidazo[2,1-b]thiazole-6-carboxylate) and compound **2** (imidazo[2,1-b]thiazole-6-carbohydrazide) were synthesized according to reported procedure [25].

Synthesis of (Z)-**N'-(3-ethoxy-2-hydroxybenzylidene)**imidazo[2,1-b]thiazole-**6- carbohydrazide (X)**. **2** (90 mg, 495 mmol) and 3-ethoxy-2-hydroxybenzaldehyde (83 mg, 500 mmol) were mixed in 15 ml ethanol and stirred at room temperature for 12 h and a pale-yellow precipitate appeared. The precipitate was filtered and then washed with ethanol (1 ml × 2) to obtain the pure pale-yellow solid **X**. Yield: 77 mg, 46%. Ms (ESI): m/z = 331.09 $[M + H]^+$, 353.07 $[M + Na]^+$. FTIR (KBr, cm^{-1}): 3314 (N-H), 1667 (C = O), 1541 (C = N). ^{1}H NMR (400 MHz, DMSO) δ 12.18 (s, 1 H), 11.30 (s, 1 H), 8.70 (s, 1 H), 8.40 (s, 1 H), 8.00 (d, J = 4.4 Hz, 1 H), 7.45 (d, J = 4.4 Hz, 1 H), 7.01 (dd, J = 7.8, 2.7 Hz, 2 H), 6.83 (t, J = 7.9 Hz, 1 H), 4.05 (q, J = 6.9 Hz, 2 H), 1.34 (t, J = 6.9 Hz, 3 H). ^{13}C NMR (101 MHz, DMSO) δ 158.46, 149.44, 149.20, 148.15, 147.52, 140.51, 122.04, 120.71, 119.41, 119.33, 117.22, 116.12, 115.81, 64.62, 15.25.

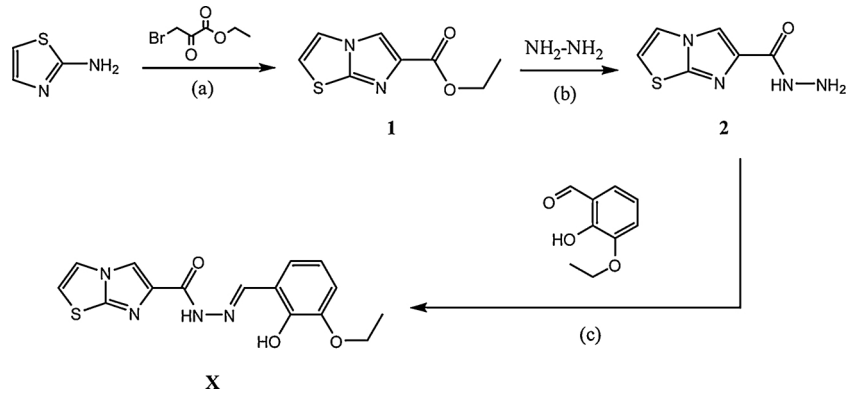

Scheme 1. Synthesis routes of **X**. Conditions: (a) THF/ethanol, 25°C/r.f., 20 h/4 h; (b) ethanol, r.t., overnight; (c) ethanol, r.t., 12 h.

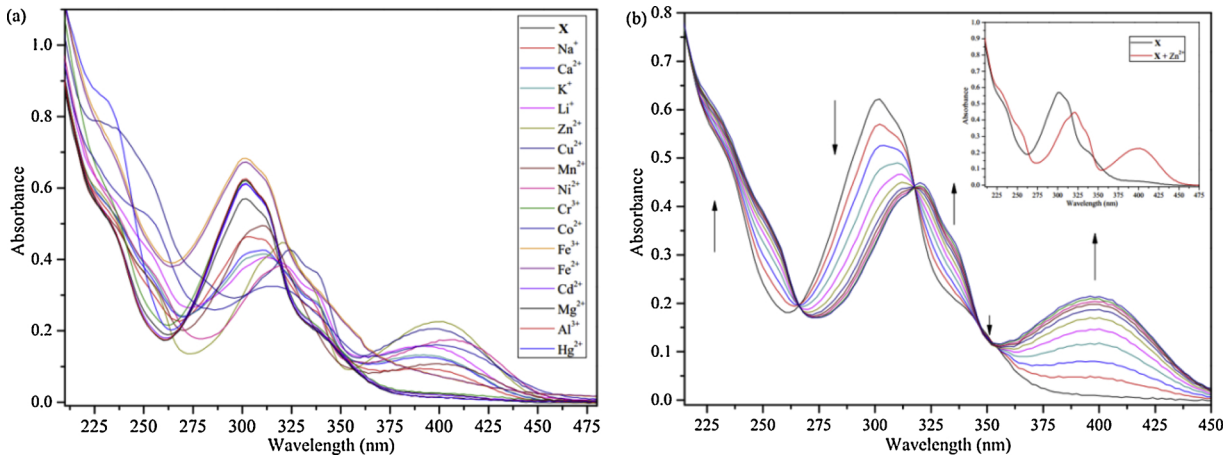

Fig. 1. (a) UV–vis spectra of **X** (1×10^{-5} M) in the presence of 6 equiv. various metal ions (Na^+, Ca^{2+}, K^+, Li^+, Zn^{2+}, Cu^{2+}, Mn^{2+}, Ni^{2+}, Cr^{3+}, Co^{2+}, Fe^{3+}, Fe^{2+}, Cd^{2+}, Mg^{2+}, Al^{3+} and Hg^{2+}) in ethanol/H_2O buffer solution (v/v = 9:1, tris = 10 mM, pH = 7.4). (b) UV–vis spectra for **X** (1×10^{-5} M) upon gradual addition of Zn^{2+} (0–6 equiv.) in ethanol/H_2O buffer solution. Inset: UV–vis spectrum of **X** and **X**[Zn^{2+}].

3. Results and discussion

As shown in Scheme 1, **X** was designed and synthesized in medium yield according to the synthetic route. Compound **1** (ethyl imidazo[2,1-b]thiazole-6-carboxylate) and compound **2** (imidazo[2,1-b]thiazole-6-carbohydrazide) were prepared according to reported procedure [25]. Compound **1** was obtained by the reaction of thiazol-2-amine with ethyl 3-bromo-2-oxopropanoate (80%) in THF solution. Then, compound **1** and hydrazide hydrate (80%) were stirred overnight in ethanol solution at room temperature to produce compound **2** as white solid. The structure of **X** was characterized by ^{1}H NMR (Fig. S1), ^{13}C NMR (Fig. S2), FTIR (Fig. S3), ESI-MS (Fig. S4). All of the data in the spectra were in good accordance with the structure.

3.1. The UV–vis spectral studies of X

In Fig. 1, the UV–vis spectral selective properties of the **X** for various metal ions (including Na^+, Ca^{2+}, K^+, Li^+, Zn^{2+}, Cu^{2+}, Mn^{2+}, Ni^{2+}, Cr^{3+}, Co^{2+}, Fe^{3+}, Fe^{2+}, Cd^{2+}, Mg^{2+}, Al^{3+} and Hg^{2+}) and the UV–vis spectral titration properties of the **X** for Zn^{2+} ions were carried out in ethanol/H_2O (v/v = 9:1) buffer solution (0.01 M tris, pH = 7.4). The experiments were carried out at a concentration of **X** was maintained at 1×10^{-5} M. As shown in Fig. 1a, the absorption band of the **X** was found at 302 nm and is of the n-π* electron transitions type. When 6 equiv. of different metal ions were added, most of them could induce significant changed in the UV–vis spectrum, that is, the absorption band at 302 nm gradually decreased and a new absorption band appeared near 400 nm. As shown in Fig. 1b, upon gradually addition of Zn^{2+} to **X** from 0 to 6 equiv., the absorption band at 302 nm gradually decreased and two absorption bands appeared at 320 nm and 400 nm. At the same time, in Fig. 1b inset, it can be clearly seen that there were four obvious isosbestic points at 356 nm, 344 nm, 318 nm and 264 nm, indicating that the **X** formed a stable complex with Zn^{2+} ions.

3.2. The fluorescence spectral studies of X

The fluorescence emission response of **X** (1×10^{-5} M) with different metal ions (6×10^{-5} M) was carried out in ethanol/H_2O (v/v = 9:1) buffer solution (0.01 M tris, pH = 7.4). As shown in Fig. 2a, **X** exhibited a low fluorescence intensity (Φ = 0.016) under excitation wavelength of 330 nm. Upon addition of various metal ions (Zn^{2+}, Li^+, Al^{3+}, Cd^{2+}, Co^{2+}, Fe^{3+}, Mg^{2+}, Cr^{3+}, Mn^{2+}, Na^+, Fe^{2+}, K^+, Cu^{2+}, Ni^{2+}, Ca^{2+} and Hg^{2+}), only Zn^{2+} could induce obvious changed in the fluorescence intensity (Φ = 0.3) at 511 nm. In Fig. 2b, after the addition of Zn^{2+} ions, the fluorescence intensity increased by 42 times, while negligible response of **X** was observed towards other metal ions. In Fig. 2c, the signal with significant fluorescence enhancement can be easily seen under the UV lamp (from colorless to yellow-green) only when Zn^{2+} ions were added, indicating that the probe had good selectivity to Zn^{2+} ions in ethanol/H_2O solution. Moreover, the fluorescence response of **X** towards Zn^{2+} ions were examined in ethanol/H_2O solution in the presence of other competitive metal ions, such as Li^+, Al^{3+}, Cd^{2+}, Co^{2+}, Fe^{3+}, Mg^{2+}, Cr^{3+}, Mn^{2+}, Na^+, Fe^{2+}, K^+, Cu^{2+}, Ni^{2+}, Ca^{2+} and Hg^{2+}. As shown in Fig. S5, except for two transition metal ions (Co^{2+} and Cu^{2+}), most of the competitive cations had little interference in the detection of Zn^{2+}. Co^{2+} and Cu^{2+} could completely quenched fluorescence of **X**[Zn^{2+}]. This may be attributed to that these two ions and probe formed fluorescent complexes with low fluorescence [27–31]. The above results showed that the sensor, **X**, could be used as a selective fluorescent sensor for Zn^{2+} even in the presence of other competitive metal ions, while it was less effective in the presence of Co^{2+} and Cu^{2+} in ethanol/H_2O buffer solution.

In order to further explore the sensing capability of **X** toward Zn^{2+} ions, the detailed fluorescence titration experiments were conducted and the experimental data were shown in Fig. 3. The free probe **X** displayed maximum fluorescence intensity at 461 nm. In Fig. 3a, with the increased of Zn^{2+} ions concentration, the fluorescence intensity of **X** was gradually enhanced. That is, in Fig. 3b, the fluorescence intensity of **X** gradually increased with the increase of Zn^{2+} ions concentration from 0 to 6×10^{-5} M and reached a plateau when the concentration of Zn^{2+} was up to 6×10^{-5} M. The fluorescence intensity had a good linear relationship ($R^2 = 0.96$) with the Zn^{2+} ions concentration from 0 to 7×10^{-8} M (Fig. 3b inset). Based on fluorescence titration data, the detection limit was determined to be 1.2×10^{-9} M according to the 3σ/s method and the association constant between **X** and Zn^{2+} was calculated to be 2.2×10^5 M^{-1} (Fig. S6) by the Benesi-Hildebrand Eq. (2). In addition, the binding ratio of **X** to Zn^{2+} were shown in Fig. S7. As a result, when the molar fraction of [Zn^{2+}] / ([X] + [Zn^{2+}]) was around 0.5, the fluorescence intensity of [X] + [Zn^{2+}] reached the maximum, indicating that the stoichiometry between **X** and Zn^{2+} was 1:1. The composition of complex had been proved by mass spectrometry analysis. The mass spectrometry results indicated that a peak at *m/z* 331.0926 corresponding to [**X** + H]$^+$ and a peak at *m/z* 353.0745 corresponding to [**X** + Na]$^+$ were observed. After addition of Zn^{2+}, a peak at *m/z* 428.9789 corresponding to [**X** + Zn^{2+} + Cl- - 2H$^+$]- was observed (Fig. S8), indicating **X**, Zn^{2+} and Cl- formed a stable ternary complex. In a word, the titration results indicated that **X** had an excellent sensitivity towards Zn^{2+} based on the fluorescence turn-on response in ethanol/H_2O buffer solution.

The effect of pH on the fluorescence of **X** in the absence and

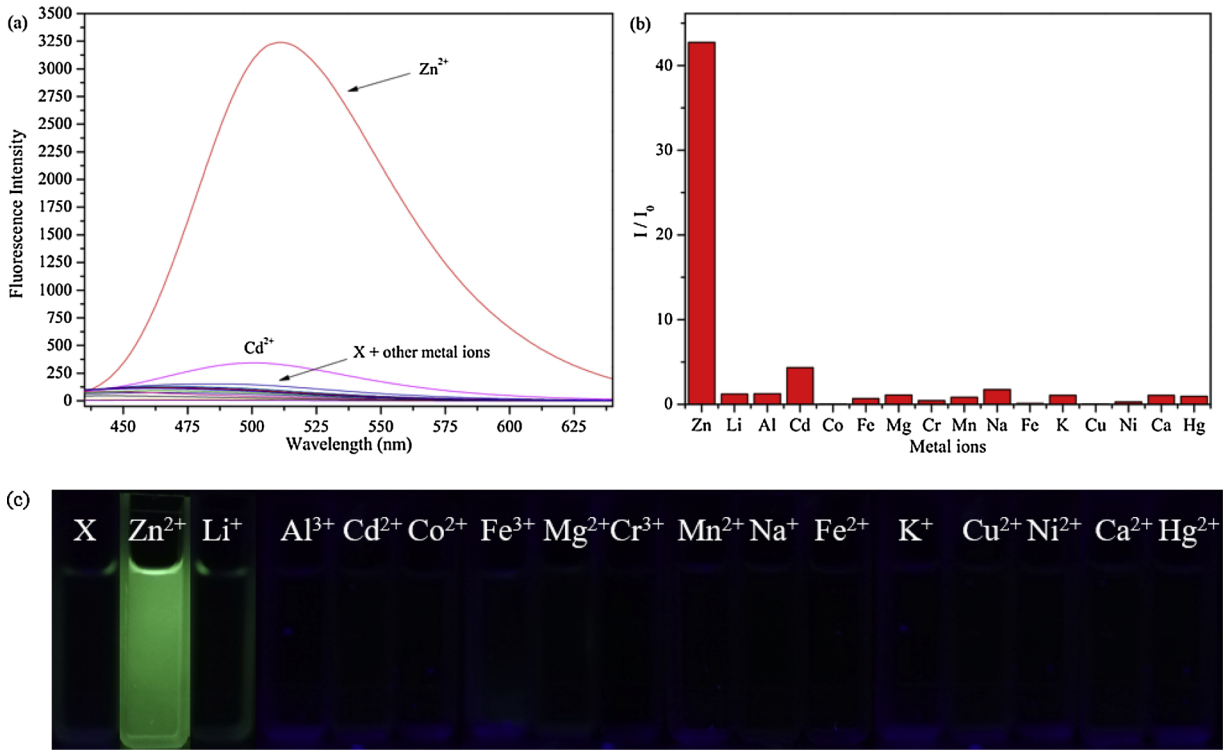

Fig. 2. (a) and (b) Fluorescence spectra of **X** (1×10^{-5} M) in the presence of 6 equiv. various metal ions (Zn^{2+}, Li^{+}, Al^{3+}, Cd^{2+}, Co^{2+}, Fe^{3+}, Mg^{2+}, Cr^{3+}, Mn^{2+}, Na^{+}, Fe^{2+}, K^{+}, Cu^{2+}, Ni^{2+}, Ca^{2+} and Hg^{2+}) in ethanol/H_2O buffer solution (v/v = 9:1, tris = 10 mM, pH = 7.4). (c) Photograph of a solution of **X** in the presence of various metal ions under UV light.

presence of Zn^{2+} was evaluated. As shown in Fig. 4, the fluorescence intensity of **X** was stable in the range of pH 2 to 7.4 and slightly increased with the change of pH values from 7.4 to 12. In addition, when addition of 6 equiv. Zn^{2+} to the tris buffer solution of probe **X** at different pH value, the fluorescence intensity of **X**[Zn^{2+}] was found to be the highest at pH 7.4. Under acidic conditions (pH < 6), **X** had no fluorescence response to Zn^{2+} ions due to the protonation of amino lead to the decrease of the coordination ability of **X** to Zn^{2+} ions. As the pH increased (6–7.4), the fluorescence intensity of **X**[Zn^{2+}] increased gradually and reached its maximum at pH 7.4. Under alkaline conditions (pH > 7.4), the fluorescence intensity of **X**[Zn^{2+}] gradually decreased with the change of pH from 7.4 to 12, which was attributed to the formation of $Zn(OH)_2$ and reduced the concentration of **X**[Zn^{2+}]. The results of pH titration indicated that the sensor could be used detection of Zn^{2+} in physiological conditions for biological samples.

3.3. The fluorescence spectral studies of X[Zn^{2+}]

In addition, the reversibility of probe was an important performance of probe. The fluorescence emission response of **X**[Zn^{2+}] with different anions (4×10^{-5} M) was carried out in ethanol/H_2O (v/v = 9:1) buffer solution (0.01 M tris, pH = 7.4). As mentioned above, the solution exhibited moderate fluorescence intensity when Zn^{2+} ions were added under excitation wavelength of 330 nm. As shown in Fig. 5a, upon addition of various anions ($Na_4P_2O_7$, NaCl, NaF, NaBr, KI, $NaNO_2$, $NaHCO_3$, Na_2S, NaS_2O_3, Na_2SO_4, $NaNO_3$, $NaHSO_3$ and $NaBF_3$), only $Na_4P_2O_7$ (PPi) could induce obvious changes in the fluorescence intensity at 511 nm. In Fig. 5b, after the addition of PPi, the fluorescence intensity was quenched by 95%, while the addition of other metal ions was quenched slightly in fluorescence intensity (NaF, NaBr, KI, NaS_2O_3, $NaNO_3$, $NaHSO_3$ and $NaBF_3$ could quenched about 10% of the

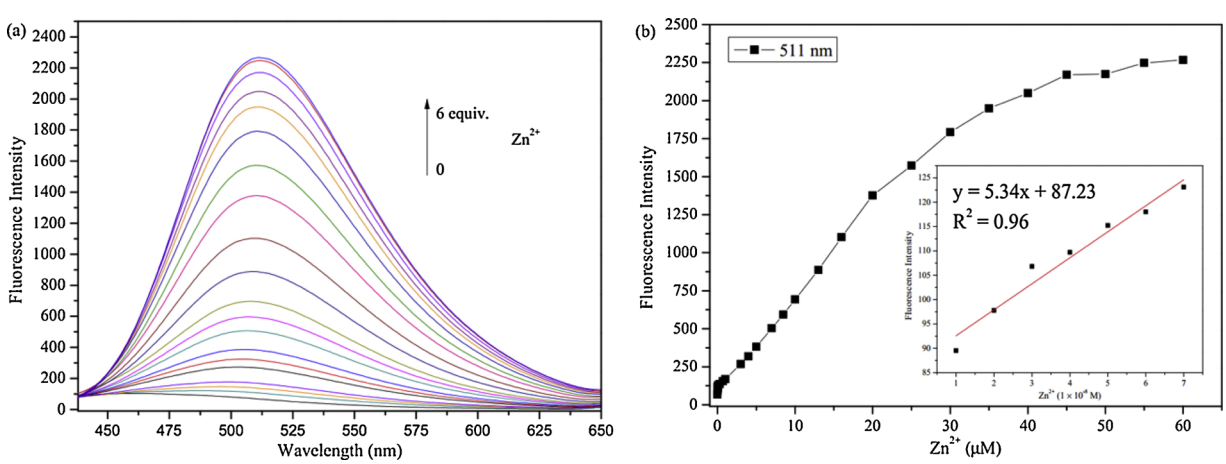

Fig. 3. (a) and (b) Fluorescence spectra of **X** (1×10^{-5} M) upon titration with Zn^{2+} (0–6 equiv.) in ethanol/H_2O buffer solution (v/v = 9:1, tris = 10 mM, pH = 7.4).

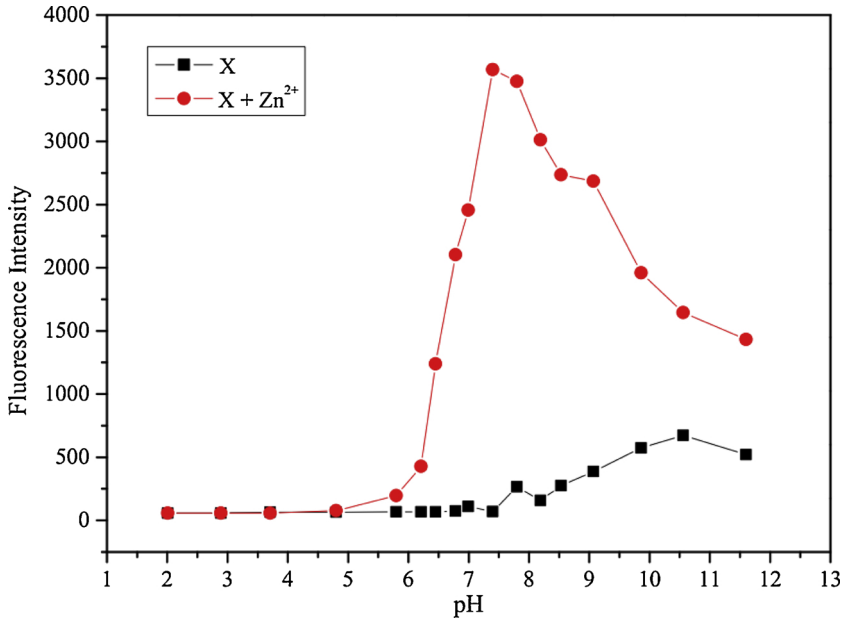

Fig. 4. Fluorescence spectra of **X** (1×10^{-5} M) at various pH values (in the absence and presence of Zn^{2+}) in ethanol/H_2O buffer solution (v/v = 9:1, tris = 10 mM).

fluorescence intensity). Interestingly, the fluorescence intensity increased slightly (15%) after the addition of NO_2-, which is attributed to the fact that NO_2- could replace the Cl- in the ternary complex to form a more stable structure and thus enhanced the fluorescence [23]. In Fig. 5c, under UV lamp, the fluorescence signal changes could be easily observed from yellow-green to colorless when PPi was added, showing good turn-off fluorescence behavior. Moreover, competitive fluorescence experiment was shown in Fig. S9. PPi was added to the solution of **X**[Zn^{2+}] in the presence of various anions, including NaCl, NaF, NaBr, KI, $NaNO_2$, $NaHCO_3$, Na_2S, NaS_2O_3, Na_2SO_4, $NaNO_3$, $NaHSO_3$ and $NaBF_3$. all anions had no effect on the fluorescence detection of PPi. These results indicated that the **X**[Zn^{2+}] had good selectivity to PPi in ethanol/H_2O solution

Moreover, the fluorescence titration experiment of **X**[Zn^{2+}] to PPi were also conducted. As shown in Fig. 6a, with the increased of PPi concentration, the fluorescence intensity of **X**[Zn^{2+}] was gradually decreased. In Fig. 6b, the fluorescence intensity of **X** gradually decreased with the increase of PPi concentration from 0 to 1.5×10^{-5} M

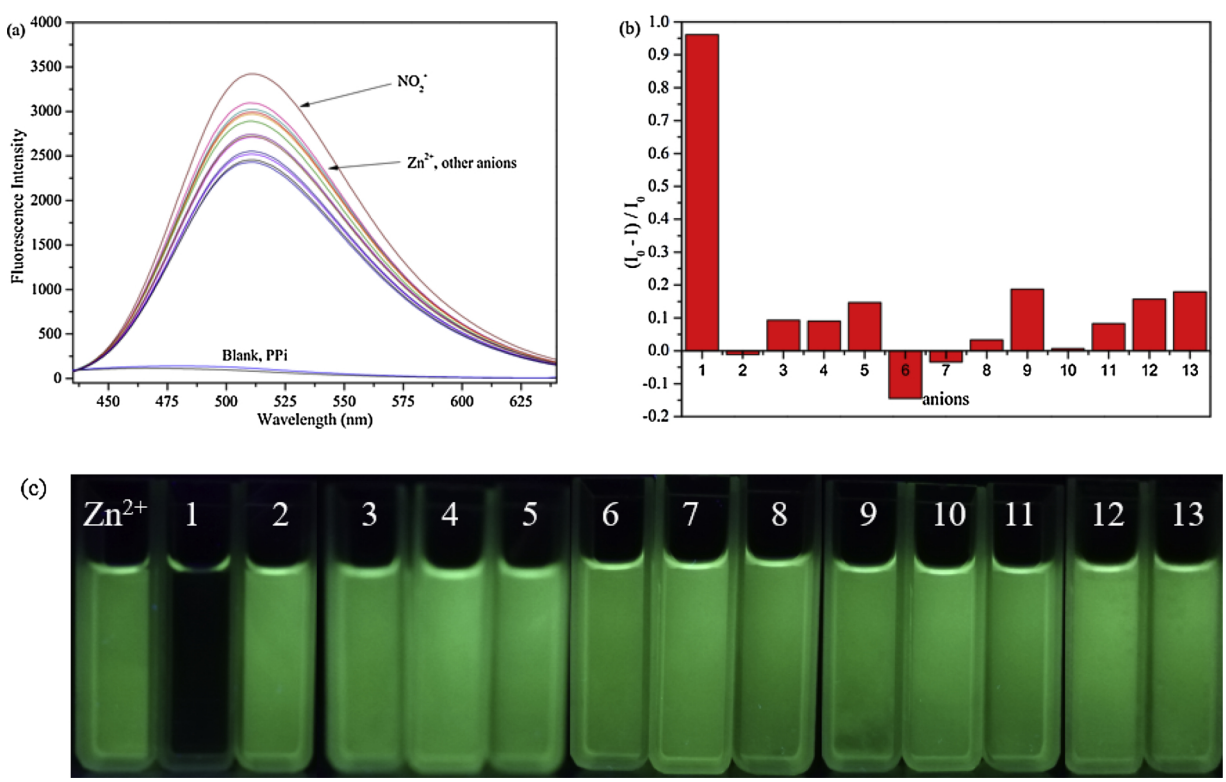

Fig. 5. (a) and (b) Fluorescence spectra of **X**[Zn^{2+}] in the presence of 4 equiv. various anions (1. $Na_4P_2O_7$, 2. NaCl, 3. NaF, 4. NaBr, 5. KI, 6. $NaNO_2$, 7. $NaHCO_3$, 8. Na_2S, 9. NaS_2O_3, 10. Na_2SO_4, 11. $NaNO_3$, 12. $NaHSO_3$, 13. $NaBF_3$) in ethanol/H_2O buffer solution (v/v = 9:1, tris = 10 mM, pH = 7.4). (c) Photograph of a solution of **X**[Zn^{2+}] in the presence of various anions under UV light.

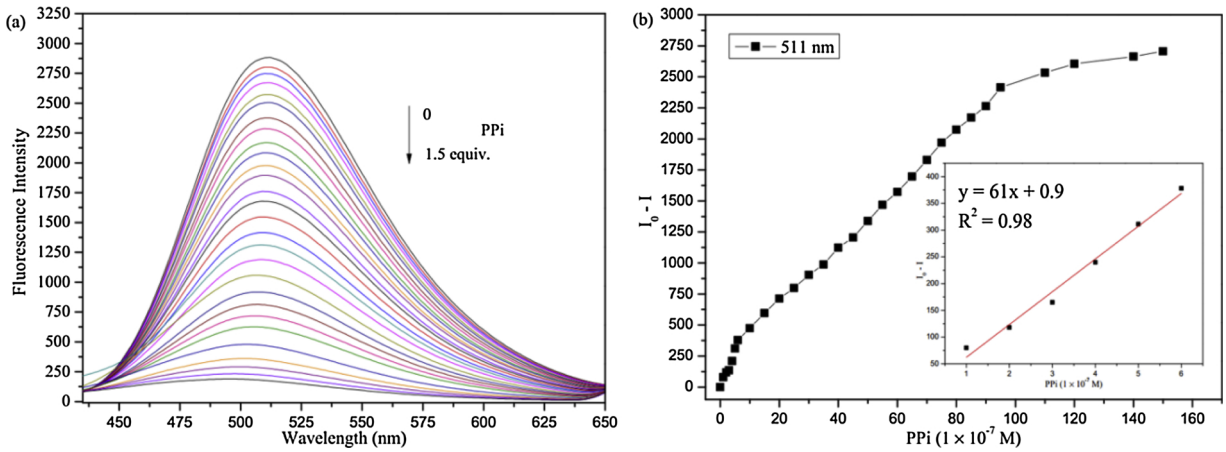

Fig. 6. (a) and (b) Fluorescence spectra of **X**[Zn^{2+}] upon titration with PPi (0–1.5 equiv.) in ethanol/H_2O buffer solution (v/v = 9:1, tris = 10 mM, pH = 7.4).

and reached a plateau when the concentration of Zn^{2+} was up to 1.5×10^{-5} M. The fluorescence intensity had a good linear relationship ($R^2 = 0.98$) with the PPi concentration from 0 to 6×10^{-7} M (Fig. 6b inset). The detection limit was determined to be 1.9×10^{-9} M according to the 3σ/s method, demonstrating that **X**[Zn^{2+}] was a highly sensitive sensor for PPi in ethanol/H_2O solution.

The reversibility experiments of **X** are shown in Fig. 7. Initially, X showed very low fluorescence intensity. When 10 equiv. Zn^{2+} ions were added, the fluorescence signal was enhanced. And then, Pyrophosphate (PPi, 6 equiv.) was added to the solution of **X**[Zn^{2+}] and then the fluorescence signal at 511 nm was immediately disappeared. Treated with Zn^{2+} again, the fluorescence of the system was recovered again. This "off-on-off" fluorescence behavior was observed by the alternative addition of Zn^{2+} and PPi to the system. What's more, after two cycles **X**[Zn^{2+}] still showed a good response toward PPi. These results indicated that the **X**[Zn^{2+}] complex with high selectivity and sensitivity could be used as a new sensor to detect PPi in ethanol/H_2O solution.

3.4. Binding mode and theoretical calculations

According to the above experimental data, the binding model of **X** to Zn^{2+} ions was also explored. Firstly, the stoichiometric ratio of **X** and Zn^{2+} was obtained as 1:1 based on B-H equation (Fig. S6) and Job's plot experiment (Fig. S7). And then, this was further exploration through mass spectrometry data (Fig. S8). The mass spectrometry results indicated that a peak at *m/z* 428.9789 corresponding to [**X** + Zn^{2+} + Cl^- - $2H^+$]$^-$ was observed when addition of $ZnCl_2$, indicating **X**, Zn^{2+} and Cl^- formed a stable ternary complex. All of the experimental data indicated that the binding ratio between **X** and Zn^{2+} ions was 1:1. Moreover, as shown in Fig. 8, oxygen (carbonyl and hydroxy) and nitrogen (N—H and CN=) were electronegative so they have strong complexation with metal ions (Fig. S10). In addition, the possible binding mechanism between **X** and Zn^{2+} ions were proposed according to experiments data and relevant literatures [32–37], as shown in Scheme 2. The hydroxy group at 3-ethoxy-2-hydroxybenzaldehyde was involved in the complexation of Zn^{2+} ions, while the ethoxy group was not involved. The nitrogen atoms on C=N bond participate in the complexation [23,32].

In order to prove the binding mechanism and fluorescence response mechanism of **X** to Zn^{2+} ions, structure optimization and energy calculation of **X** and **X**[Zn^{2+}] were investigated using *ab initio* density functional theory (DFT) combined with time-dependent density functional theory (TDDFT) calculations, as implemented in the Gaussian 09

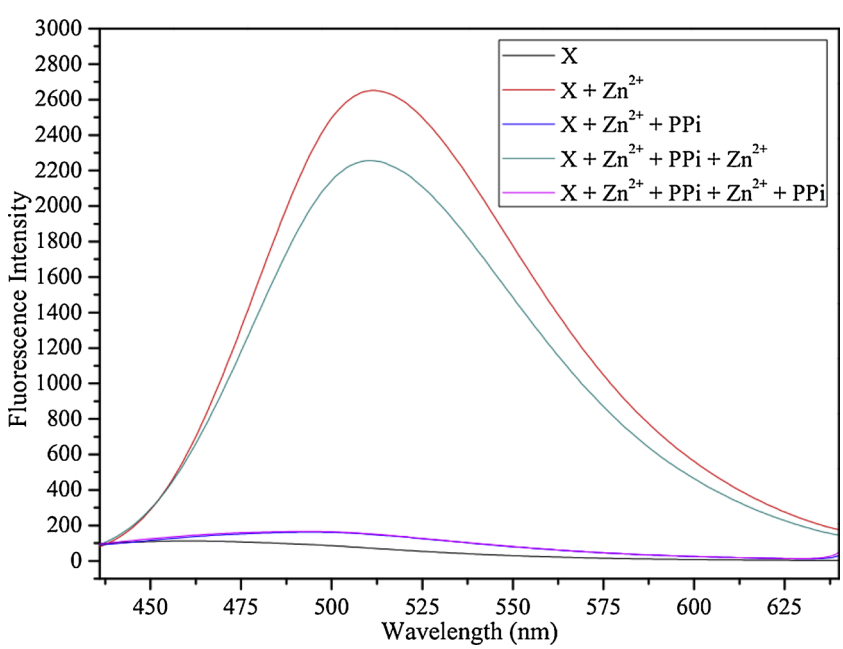

Fig. 7. Reversible switching of the emission of **X** by repeated addition of Zn^{2+} and PPi in ethanol/H_2O buffer solution (v/v = 9:1, tris = 10 mM, pH = 7.4).

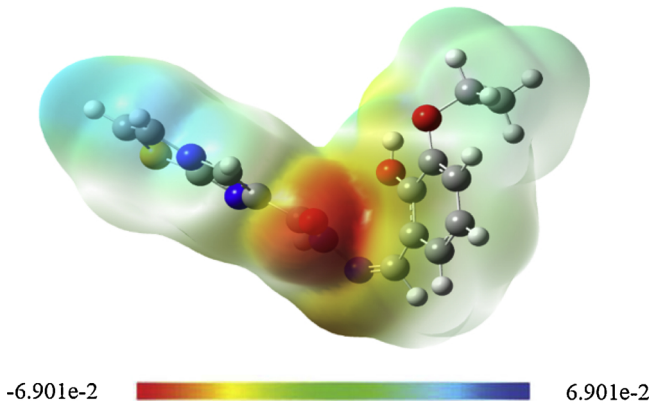

Fig. 8. Electrostatic potential coloring of the molecular surface of the **X**. where the light-gray, red, blue, white, yellow atoms denote C, O, N, H, S atoms, respectively.

package based on B3LYP/6-31 G(d) basis [38]. As shown in Fig. S11, the optimal structure of **X** and **X**[Zn^{2+}] were obtained by gauss calculations. For **X**, the imidazo[2,1-*b*]thiazole (fluorescence nuclei) and 3-ethoxy-2-hydroxybenzaldehyde (fluorescence receptor) part maintained a good planar property, respectively, and their dihedral angle was about 68.18 degrees. After binding with Zn^{2+} ions, the dihedral angle between the fluorescence nuclei and receptor becomes 7.1 degrees, indicating that the planar nature of the whole **X**[Zn^{2+}] molecule increased.

In addition, the spatial distributions and orbital energies of the highest occupied molecular orbital (HOMO) and the lowest unoccupied molecular orbital (LUMO) of **X** and **X**[Zn^{2+}] complexes were also exhibited in Fig. 9. For free **X**, the highest occupied molecular orbital (HOMO) was mostly distributed over 3-ethoxy-2-hydroxybenzaldehyde (fluorescence receptor) and imine (C=N) groups whereas the lowest unoccupied molecular orbital (LUMO) charge density was uniformly distributed over the whole probe molecule [39]. There was partial electron transfer in the excited, so **X** showed very weak fluorescence. After binding with Zn^{2+} ions, the HOMO was still around the receptor and C=N groups, while electrons in LUMO are mostly localized on the fluorophore [40]. Moreover, the energy gap of **X** and **X**[Zn^{2+}] were also calculated to be 4.55 and 3.22, respectively. The results showed that the role of Zn^{2+} ions was to increased the degree of intramolecular charge transfer, enhanced the planarity and rigidity of the whole molecule. This observation additionally supported the role of inhibition of photo-induced electron transfer (PET) along with the chelation enhanced fluorescence mechanism (CHEF) effect for the fluorescence enhancement [5,18,33,40,41]. The calculated results and experimental phenomena were highly consistent with the theoretical basis.

3.5. Logic gate behavior of X

The fluorescence behavior of **X** at 511 nm mimics the INHIBIT logic gate, the circuit and the truth table for the INHIBIT logic gate were shown in Fig. 10 [42]. In Fig. 10a, the INHIBIT logic gate was an "AND" gate with an inverter in one of its input and had two input signals and an output signal [43]. The emission intensity of **X** at 511 nm was regarded as an initial value. The fluorescent intensity output value ($I_{f\ 511\ nm}$) below the threshold level were assigned as logic "0", while the output values above the threshold were assigned as logic "1" [44]. In Fig. 10b, the output was only logic "1" when the input signal was (IN1 = 1 and IN2 = 0). While in other input forms (IN1 = 0 and IN2 = 0, IN1 = 0 and IN2 = 1, IN1 = 1 and IN2 = 1), the output signals were all logic "0" [45]. That is, the fluorescence intensity of **X** was weak. After addition of Zn^{2+} ions, the fluorescence enhancement. However, the fluorescence intensity was low in the presence of Cu^{2+} or Co^{2+}. When Zn^{2+} and Cu^{2+} or Co^{2+} coexist, the fluorescence intensity of the system remained low. In Fig. 10c, the algorithm was similar to the one above. The system fluorescence was observed in the presence of Zn^{2+} ions alone and disappeared in the presence of PPi. Thus, this behavior was very consistent with INHIBITORY logic gates [46].

4. Conclusions

In summary, A novel simple schiff base fluorescent sensor, **X**, was designed and synthesized based on 3-ethoxy-2-hydroxybenzaldehyde as the receptor and imidazo[2,1-*b*]thiazole-6-carboxylic acid as the fluorophore. **X** showed excellent sensitivity and selectivity for Zn^{2+} by exhibiting a large fluorescence enhancement (about 42 times) with distinct color changed from colorless to yellow-green under UV light, whereas other competitive metal ions did not show any noticeable change. Conversely, the fluorescence of the **X**[Zn^{2+}] complex was reduced by the addition of PPi, confirming that the recognition process was reversible. In general, **X** could act as a fluorescence probe for the sequential detection of Zn^{2+} and PPi and the detection limit was 1.2×10^{-9} M and 1.9×10^{-9} M, respectively. The binding ratio of the **X** and Zn^{2+} was 1:1 confirmed by mass spectral analysis and Job's plot. The binding mode and sensing mechanism of **X** with Zn^{2+} was verified by DFT/TDDFT calculations using Gaussian 09. Additionally, an INHIBIT logic gates had been successfully designed and constructed. In addition, a series of other schiff base fluorescent sensors had already designed and synthesized in our lab and their optical properties and practical applications will be studied.

Acknowledgements

The authors thank the Henan Sanmenxia Aoke Chemical Industry Co., Ltd. w0920 for financial support. Financial support by the National Natural Science Foundation of China (Grants 21708013) and the China Postdoctoral Science Foundation (Grants 2017M620288)

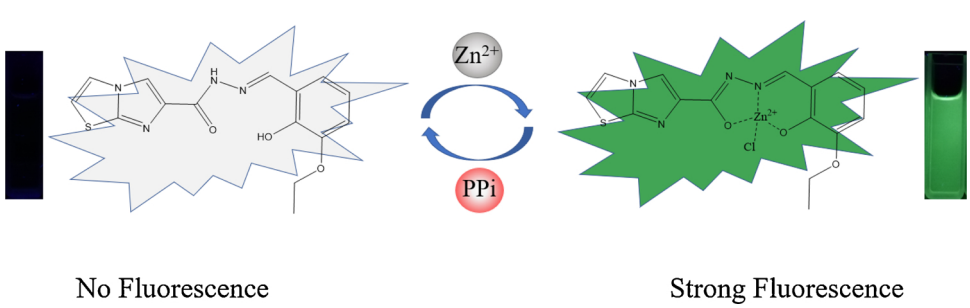

Scheme 2. The proposed binding mode of **X** with Zn^{2+}.

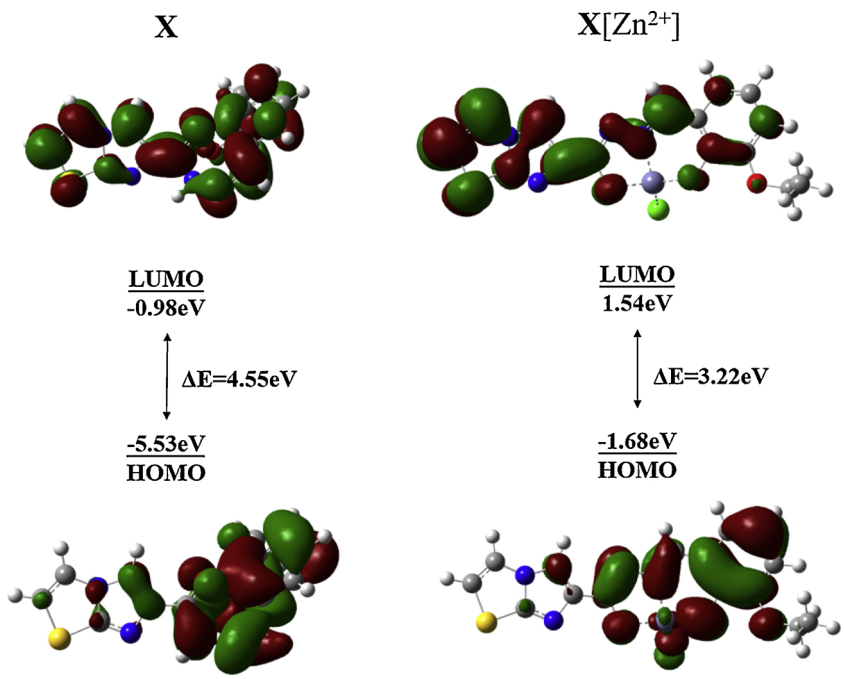

Fig. 9. Energy diagram of HOMO and LUMO orbital **X** and **X**[Zn^{2+}].

(a)

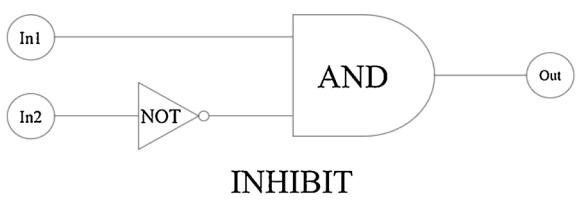

(b)

IN1 (Zn^{2+})	IN2 (Cu^{2+} or Co^{2+})	OUT ($I_{f511\ nm}$)
0	0	0
1	0	1
0	1	0
1	1	0

(c)

IN1 (Zn^{2+})	IN2 (PPi)	OUT ($I_{f511\ nm}$)
0	0	0
1	0	1
0	1	0
1	1	0

Fig. 10. Operation of the INHIBIT logic gate. (a) INHIBIT logic scheme. (b) Truth table for the INHIBIT logic gate.

Appendix A. Supplementary data

Supplementary material related to this article can be found, in the online version, at doi:https://doi.org/10.1016/j.jphotochem.2019.112026.

References

[1] X. Feng, Y. Fu, J. Jin, J. Wu, A highly selective and sensitive fluorescent sensor for relay recognition of Zn^{2+} and HSO^{4-}/H_2PO^{4-} with "on-off" fluorescent responses, Anal. Biochem. 563 (2018) 20–24.
[2] J. Yan, L. Fan, J. Qin, C. Li, Z. Yang, A novel and resumable Schiff-base fluorescent chemosensor for Zn(II), Tetrahedron Lett. 57 (2016) 2910–2914.
[3] L. Nyiranshuti, D.P. Kennedy, A.G. DiPasquale, A.L. Rheingold, R.P. Planalp, TAMEisoquin, a novel tripodal fluorescent zinc sensor with high Zn(II) affinity and Zn(II)/Cd(II) selective fluorescence response: synthesis, coordination geometry, spectroscopy, and comparative response to biometal ions, Polyhedron 109 (2016) 147–153.
[4] J. Qin, L. Fan, Z. Yang, A small-molecule and resumable two-photon fluorescent probe for Zn^{2+} based on a coumarin Schiff-base, Sens. Actuators B 228 (2016) 156–161.
[5] Z. Lu, W. Fan, Y. Lu, C. Fan, H. Zhao, K. Guo, W. Chua, Y. Lu, A highly sensitive fluorescent probe for bioimaging zinc ion in living cells and zebrafish models, New J. Chem. 42 (2018) 12198–12204.
[6] L. Tang, D. Wu, Z. Huang, Y. Bian, A fluorescent sensor based on binaphthol-quinoline Schiff base for relay recognition of Zn^{2+} and oxalate in aqueous media, J. Chem. Sci. 128 (2016) 1337–1343.
[7] Y. Tang, Y. Huang, L. Lu, C. Wang, T. Sun, J. Zhu, G. Zhu, J. Pan, Y. Jin, A. Liu, M. Wang, Synthesis of a new pyrene-devived fluorescent probe for the detection of Zn^{2+}, Tetrahedron Lett. 59 (2018) 3916–3922.
[8] T. Mandal, A. Hossain, A. Dhara, A.A. Masum, S. Konar, S.K. Manna, S.K. Seth, S. Pathak, S. Mukhopadhyay, Terpyridine derivatives as "turn-on" fluorescence chemosensors for the selective and sensitive detection of Zn^{2+} ions in solution and in live cells, Photochem. Photobiol. Sci. 17 (2018) 1068–1074.
[9] J. Qin, B. Wang, Z. Yang, K. Yu, A ratiometric fluorescent chemosensor for Zn^{2+} in aqueous solution through an ESIPT coupled AIE process, Sens. Actuators B 224 (2016) 892–898.
[10] H. Wang, T. Kang, X. Wang, L. Feng, A facile strategy for achieving high selective Zn (II) fluorescence probe by regulating the solvent polarity, Talanta 184 (2018) 7–14.
[11] A.K. Mahapatra, S.K. Manna, C.D. Mukhopadhyay, D. Mandal, Pyrophosphate-selective fluorescent chemosensor based on ratiometric tripodal-Zn(II) complex: application in logic gates and living cells, Sens. Actuators B 200 (2014) 123–131.
[12] M. Guo, P. Dong, Y. Feng, X. Xi, R. Shao, X. Tian, B. Zhang, M. Zhu, X. Meng, A two-photon fluorescent probe for biological Cu (II) and PPi detection in aqueous solution and in vivo, Biosens. Bioelectron. 90 (2017) 276–282.
[13] Y. Xia, H. Zhang, X. Zhu, Q. Zhang, M. Fang, X. Li, H. Zhou, X. Yang, X. Zhang, Y. Tian, Two-photon fluorescent probe with enhanced absorption cross section for relay recognition of $Zn^{2+}/P_2O_7^{4-}$ and in vivo imaging, Spec. Acta Part A: Mol. 204 (2018) 446–451.
[14] J.H. Kang, J. Han, H. Lee, M.H. Lim, K.T. Kim, C. Kim, A water-soluble fluorescence chemosensor for the sequential detection of Zn^{2+} and pyrophosphate in living cells and zebrafish, Dyes Pigm. 152 (2018) 131–138.
[15] T. Wei, F. Wang, Y. Chen, J. Qiang, Z. Zhang, T. Chen, X. Chen, A fluorescence probe for bisulfite sensing based on the bisulfite-induced binding site transfer between Zn^{2+} and an aminoquinoline derivate, Dyes Pigm. 159 (2018) 322–330.
[16] W. Gao, Y. Zhang, H. Li, S. Pu, A multi-controllable selective fluorescent turn-on chemosensor for Al^{3+} and Zn^{2+} based on a new diarylethene with a 3-(4-methylphenyl)-1H-pyrazol-5-amine Schiff base group, Tetrahedron 74 (2018) 6299–6309.
[17] Z. Wang, S. Cui, S. Qiu, Z. Zhang, S. Pu, A highly sensitive fluorescent sensor for Zn^{2+} based on diarylethene with an imidazole unit, Spec. Acta Part A: Mol. 205 (2018) 21–28.
[18] H. Liu, T. Liu, J. Li, Y. Zhang, J. Li, J. Song, J. Qu, W.Y. Wong, A simple Schiff base as dual-responsive fluorescent sensor for bioimaging recognition of Zn^{2+} and Al^{3+} in living cells, J. Mater. Chem. B 6 (2018) 5435–5442.
[19] M. Patil, K. Keshav, M.K. Kumawat, S. Bothra, S.K. Sahoo, R. Srivastava, J. Rajput,

R. Bendre, A. Kuwar, Monoterpenoid derivative based ratiometric fluorescent chemosensor for bioimaging and intracellular detection of Zn^{2+} and Mg^{2+} ions, J. Photochem. Photobiol. A: Chem. 364 (2018) 758–763.
[20] A. Kim, J.H. Kang, H.J. Jang, C. Kim, Fluorescent detection of Zn(II) and In(III) and colorimetric detection of Cu(II) and Co(II) by a versatile chemosensor, J. Ind. Eng. Chem. 65 (2018) 290–299.
[21] J. Zhu, Y. Zhang, Y. Chen, T. Sun, Y. Tang, Y. Huang, Q. Yang, D. Ma, Y. Wang, M. Wang, A Schiff base fluorescence probe for highly selective turn-on recognition of Zn^{2+}, Tetrahedron Lett. 58 (2017) 365–370.
[22] J. Li, Y. Chen, T. Chen, J. Qiang, Z. Zhang, T. Wei, W. Zhang, F. Wang, X. Chen, A benzothiazole-based fluorescent probe for efficient detection and discrimination of Zn^{2+} and Cd^{2+}, using cysteine as an auxiliary reagent, Sens. Actuators B 268 (2018) 446–455.
[23] Z. Liu, C. Peng, Y. Wang, M. Pei, G. Zhang, A fluorescent sensor for Zn^{2+} and NO^{2-} based on the rational control of C = N isomerization, Org. Biomol. Chem. 14 (2016) 4260–4266.
[24] Y. Liang, L. Diao, R. Wang, N. Wang, S. Pu, A bifunctional probe for Al^{3+} and Zn^{2+} based on diarylethene with an ethylimidazo[2,1-b]thiazole-6-hydrazide unit, Tetrahedron Lett. 60 (2019) 106–112.
[25] J.A. Kaizerman, M.I. Gross, Y. Ge, S. White, W. Hu, J.X. Duan, E.E. Baird, K.W. Johnson, R.D. Tanaka, H.E. Moser, R.W. Burli, DNA binding ligands targeting drug-resistant Bacteria: structure, activity, and pharmacology, J. Med. Chem. 46 (2003) 3914–3929.
[26] M.J. Frisch, G.M. Trucks, H.B. Schlegel, G.E. Scuseria, M.A. Robb, J.R. Cheeseman, et al., GAUSSIAN 09 (Revision D.02), Gaussian Inc., Pittsburg, PA, 2006.
[27] X. Bai, J. Yan, J. Qin, Z. Yang, A multi-ion fluorescent probe for Mg^{2+}/Zn^{2+} based on a novel chromonedendron Schiff base, Inorganica Chim. Acta 474 (2018) 44–50.
[28] K. Boonkitpatarakul, A. Smata, K. Kongnukool, S. Srisurichan, K. Chainok, M. Sukwattanasinitt, An 8-aminoquinoline derivative as a molecular platform for fluorescent sensors for Zn(II) and Cd(II) ions, J. Lumin. 198 (2018) 59–67.
[29] N.A. Bumagina, E.V. Antina, A.Y. Nikonova, M.B. Berezin, A.A. Ksenofontov, A.I. Vyugin, A new sensitive and selective off-on fluorescent Zn^{2+} chemosensor based on 3,3′,5,5′-Tetraphenylsubstituted dipyrromethene, J. Fluoresc. 26 (2016) 1967–1974.
[30] F. Yu, X. Guo, X. Tian, L. Jia, A ratiomeric fluorescent sensor for Zn^{2+} based on N,N′-Di(quinolin-8-yl)oxalamide, J. Fluoresc. 27 (2017) 723–728.
[31] Y.P. Zhang, Q.H. Xue, Y.S. Yang, X.Y. Liu, C.M. Ma, J.X. Ru, H.C. Guo, A chromene pyrazoline derivatives fluorescent probe for Zn^{2+} detection in aqueous solution and living cells, Inorganica Chim. Acta 479 (2018) 128–134.
[32] W. He, Z. Liu, A fluorescent sensor for Cu^{2+} and Fe^{3+} based on multiple mechanisms, RSC Adv. 6 (2016) 59073–59080.
[33] S. Xiao, Z. Liu, J. Zhao, M. Pei, G. Zhang, W. He, A novel fluorescent sensor based on Imidazo[1,2-a]pyridine for Zn^{2+}, RSC Adv. 6 (2016) 27119–27125.
[34] J. Sun, Z. Liu, Y. Wang, S. Xiao, M. Pei, X. Zhao, G. Zhang, A fluorescence chemosensor based on imidazo[1,2-a]quinoline for Al^{3+} and Zn^{2+} in respective solutions, RSC Adv. 5 (2015) 100873–100878.
[35] M. Kumar, A. Kumar, M.H. Faizi, S. Kumar, M.K. Singh, S.K. Sahu, S. Kish, R.P. John, A selective 'turn-on' fluorescent chemosensor for detection of Al^{3+} in aqueous medium: experimental and theoretical studies, Sens. Actuators B 260 (2018) 888–899.
[36] J.Y. Yun, T.G. Jo, J. Han, H.J. Jang, M.H. Lim, C. Kim, A highly sensitive and selective fluorescent chemosensor for the sequential recognition of Zn^{2+} and S^{2-} in living cells and aqueous media, Sens. Actuators B 255 (2018) 3108–3116.
[37] H. Liu, Y. Tan, Q. Dai, H. Liang, J. Song, J. Qu, W.Y. Wong, A simple amide fluorescent sensor based on quinoline for selective and sensitive recognition of zinc (II) ions and bioimaging in living, Dyes Pigm. 158 (2018) 312–318.
[38] Y. Xu, X. Liu, J. Zhao, H. Wang, Z. Liu, X. Yang, M. Pei, G. Zhang, A new "ON-OFF-ON" fluorescent probe for sequential detection of Fe^{3+} and PPi based on 2-pyridin-2-ylethanamine and benzimidazo[2,1-a]-benz[de]isoquinoline-7-one-12-carboxylic acid, New J. Chem. 43 (2019) 474–480.
[39] C. Patra, C. Sen, A.D. Mahapatra, D. Chattopadhyay, A. Mahapatra, C. Sinha, Pyridylthioether-hydroxycoumarin Schiff base as selective Zn^{2+} fluorescence sensor, application in life cell imaging and uses of resulting complex as secondary probe for ATP sensing, J. Photochem. Photobiol. A: Chem. 341 (2017) 97–107.
[40] T. Anand, A.K. SK, S.K. Sahoo, Vitamin B6 Cofactor Derivative: A Dual Fluorescent Turn-On Sensor to Detect Zn^{2+} and CN^{-} Ions and Its Application in Live Cell Imaging, ChemistrySelect 2 (2017) 7570–7579.
[41] M. Sohrabi, M. Amirnasr, H. Farrokhpour, S. Meghdadi, A single chemosensor with combined ionophore/fluorophore moieties acting as a fluorescent "Off-On" Zn^{2+} sensor and a colorimetric sensor for Cu^{2+}: experimental, logic gate behavior and TD-DFT calculations, Sens. Actuators B 250 (2017) 647–658.
[42] X. Tian, X. Guo, F. Yu, L. Jia, An oxalamidoquinoline-based fluorescent sensor for selective detection of Zn^{2+} in solution and living cells and its logic gate behavior, Sens. Actuators B 232 (2016) 181–187.
[43] S. Wang, L. Zang, L. Zhao, X. Wang, Q. Hou, S. Jiang, A molecular half-subtractor with Zn^{2+} and UV-light as inputs, Spec. Acta Part A 77 (2010) 226–231.
[44] Y. Fu, C. Fan, G. Liu, S. Cui, S. Pu, A highly selective and sensitive ratiometric fluorescent chemosensor for Zn^{2+} based on diarylethene with a benzyl-linked 8-aminoquinoline-2-aminomethylpyridine unit, Dyes Pigm. 126 (2016) 121–130.
[45] N.N. Li, Y.Q. Ma, S. Zeng, Y.T. Liu, X.J. Sun, Z.Y. Xing, A highly selective colorimetric and fluorescent turn-on chemosensor for Zn^{2+} and its logic gate behavior, Synth. Met. 232 (2017) 17–24.
[46] N. Roy, A. Dutta, P. Mondal, P.C. Paul, T.S. Singh, Coumarin based fluorescent probe for colorimetric detection of Fe^{3+} and fluorescence turn on-off response of Zn^{2+} and Cu^{2+}, J. Fluoresc. 27 (2017) 1307–1321.